RSC Advances

PAPER

View Article Online
View Journal | View Issue

Cite this: *RSC Adv.*, 2021, **11**, 30195

The first amorphous and crystalline yttrium lactate: synthesis and structural features†

A. D. Yapryntsev,[a] A. E. Baranchikov,[a] A. V. Churakov,[a] G. P. Kopitsa,[bc] A. A. Silvestrova,[ad] M. V. Golikova,[ae] O. S. Ivanova,[a] Yu. E. Gorshkova[fg] and V. K. Ivanov*[ad]

Received 4th August 2021
Accepted 2nd September 2021

DOI: 10.1039/d1ra05923h

rsc.li/rsc-advances

The synthesis and crystal structure of the first molecular yttrium lactate complex, $Y(Lac)_3(H_2O)_2$, is reported, where the coordination sphere of yttrium is saturated with lactate ligands and water molecules, resulting in a neutral moiety. In $Y(Lac)_3(H_2O)_2$, hydrogen bonding between α-hydroxy groups and water molecules allows for the formation of 2D layers. A subtle variation in synthetic conditions, *i.e.* a slight increase in pH (5.5 instead of 4.5) promoted the formation of a semi-amorphous fibrous material with a presumed chemical composition of $Y_4(OH)_5(C_3H_5O_3)_7 \cdot 6H_2O$. The flattened fibres in this material are responsible for its good flexibility and foldability.

Introduction

Metal carboxylates attract a great deal of attention due to the wide range of their practically important properties, including high catalytic and photocatalytic activity, gas storage and sensing.[1] Their well-pronounced luminescence, enhanced by aromatic antenna ligands and high chemical stability under UV-irradiation, is of primary importance for the construction of light-emitting devices.[2,3] The design of novel metal carboxylates enables molecular magnets, low-temperature cooling agents, sorbents for gas separation, bioactive materials, *etc.*[4–10]

The functional properties of metal carboxylates are governed by their coordination chemistry, *e.g.* by the coordination ability of a central atom and the coordination mode of ligands. In d-metal complexes, carboxylate ligands usually manifest a monodentate nature, often playing the role of bridging moieties.[11,12] In contrast to d-metal carboxylates, in REE carboxylates, R–COO ligands show much more versatile coordination modes, including mono-, bi- or tridentate non-bridging and di- or trinuclear bridging modes. The relatively large size of REEs compared to 3d metals makes the 4-member chelating ring more stable than in 3d metal carboxylates, which favours the bidentate coordination of the ligands.[11] Being hard Lewis base donors, carboxylic acids are the most suitable ligands to fill the coordination sphere of REEs.[3] In turn, the large coordination numbers of REEs (6–9) (ref. 13) provide the rich coordination chemistry of REE carboxylates, demonstrating a wide variety of 1D, 2D and 3D networked coordination polymers with abundant coordination behaviours, an adjustable structure and high chemical stability.[11,14]

Functionalised carboxylic acids, including hydroxy carboxylic or amino acids, due to their potentially higher denticity and their ability to act as bridging ligands and to possibly form interligand hydrogen bonds, provide additional opportunities for the design of REE coordination compounds, including molecular complexes and MOFs.[15,16] For example, many amino-substituted organic acids have been proposed as the ligands for gadolinium ions in the construction of new contrast-enhancing agents in clinical MRI.[17,18] The coordination of lanthanides with amino acids has also been investigated in the context of creating artificial nucleases which catalyse the hydrolytic cleavage of DNA and RNA, as the coordination of peptide linkages with the metal ion affects the enzyme structure and governs its conformation.[19]

Among the substituted carboxylic acid residues, lactate (Lac) is a representative essential oxyanion that is involved in many metabolic interactions in living organisms. Lactate ions have been suggested to play an important role in the communication between cells.[20] The detection of lactate is of prime importance in the diagnosis of cancer, diabetes, stroke, heart diseases *etc.*[21] On the other hand, lactic acid-containing systems have been studied extensively as the tools for extraction and separation of rare earths and actinides within a TALSPEAK (Trivalent

[a]*Kurnakov Institute of General and Inorganic Chemistry of the Russian Academy of Sciences, Moscow, Russia. E-mail: van@igic.ras.ru*

[b]*Petersburg Nuclear Physics Institute of National Research Centre "Kurchatov Institute", St. Petersburg, Russia*

[c]*Grebenshchikov Institute of Silicate Chemistry of the Russian Academy of Sciences, St. Petersburg, Russia*

[d]*National Research University Higher School of Economics, Moscow, Russia*

[e]*Mendeleev University of Chemical Technology, Moscow, Russia*

[f]*Frank Laboratory of Neutron Physics, Joint Institute for Nuclear Research, Dubna, Russia*

[g]*Institute of Physics, Kazan Federal University, Kazan, Russia*

† Electronic supplementary information (ESI) available. CCDC 2085515. For ESI and crystallographic data in CIF or other electronic format see DOI: 10.1039/d1ra05923h

Actinide–Lanthanide Separation by Phosphorus reagent Extraction from Aqueous Komplexes) process.[22–25]

Thus, comprehensive information on lanthanide lactates is highly important in the search for new biosensors and theranostic agents, as well as for the improvement of industrial extraction processes. Unsurprisingly, the thermodynamic features of rare earth lactate complexes (formation constants, *etc.*) were the subject of extensive study during the 1960s and 1970s.[25–34] These studies resulted in the identification of several structures of lanthanide lactate moieties which can form in solutions and can presumably exist in crystalline lanthanide lactates. One unexpected result of the literature survey was that information on crystalline lanthanide lactates is extremely scarce, with the following compounds reported to date: $[LnNa(Lac)_4]\cdot 2H_2O$ (Ln = Sm, Eu),[35], $[Ln(Lac)_2](H_2O)_2\cdot ClO_4$ (Ln = Eu, Tb),[36,37] $La_4(HL)_5(Lac)_2(i\text{-}PrOH)_2(DMF)_2\cdot(7DMF + 5H_2O)$ (H_3L = 5-hydroxyisophthalic acid),[38] $Ln(TACD)(Lac)(CF_3SO_3)_2\cdot 3H_2O$ (Ln = Yb, Ho; TACD = tetraazacyclododecane-based ligand),[39] $Ln_3Ag_4(Lac)_2(IN)_8(H_2O)_5\cdot 2(ClO_4)\cdot 2.5(H_2O)$ [Ln = La, Lu; HIN = isonicotinic acid], $Sm_3Ag_4(Lac)_2(IN)_8(H_2O)_4\cdot 2(ClO_4)\cdot 2.5(H_2O)$, and $Eu_2Ag_3(S\text{-}Lac)(IN)_6(H_2O)_4\cdot 2(ClO_4)\cdot 4(H_2O)$,[40] Ln(Lac)[15MC$_{Cu^{II}Glyha}$-5]$Cl_2$ (Ln = La, Y, Ce, Pr, Nd, Sm, Eu, Gd, Tb, or Dy; 15MC$_{Cu^{II}Glyha}$-5 = copper(II)-glycinehydroximate 15-metallacrown-5 ligand).[41] As expected, in known REE lactates, a lactate ligand shows a predominantly bidentate coordination mode;[39–41] in some cases, the hydroxy group is also included in the coordination environment of a lanthanide.[38,40] A lactate ligand tends to act as a bridge connecting two,[40] or even three,[38] rare earth ions. Interestingly, examples of other rare earth α-hydroxy carboxylates are even more limited, *e.g.* the structure of lanthanide 2-hydroxy isobutyrates was described by Chen *et al.*[42]

Note that none of the known crystalline rare earth lactates can be regarded as a neutral molecular lactate complex, where the coordination sphere of a REE is saturated only with lactate ligands and water molecules resulting in a neutral molecular moiety. This fact seems to be somewhat odd, since the existence of such molecular complexes was recently predicted.[33] In their most recent paper, Roy *et al.* commented on this fact as follows: 'While lanthanide lactate complexes have been known for some time, there are no crystal structures of the isolated species to compare our optimized structures'.[33]

In order to fill the gap in rare earth lactate chemistry, the aim of the current research was to synthesise an yttrium lactate containing no additional organic ligands. When planning the synthetic strategy, account was taken of some recently reported principles in rare earth carboxylate chemistry, namely the importance of high ligand-to-metal molar ratio,[11] as well as the use of mild hydrothermal conditions facilitating the formation of REE complexes with polydentate substituted carboxylates.[36,37,43] Special attention was paid to avoid resinification reactions. This strategy enabled the preparation of the first molecular yttrium lactate, while a subtle increase in pH resulted in a semi-amorphous basic yttrium lactate, which revealed an unusual 1D shape of the particles.

Materials and methods

Materials

Yttrium chloride hexahydrate (99.9%, Lanhit), L-lactic acid (HLac, 80%, Sigma) and hexamethylenetetramine (HMT, 99+%, Alfa Aesar) were used without further purification.

Synthesis of yttrium lactates

60 ml of aqueous clear solution of yttrium chloride hexahydrate (1.7×10^{-2} M), HMT (2.4, 5.6 or 12×10^{-2} M) and L-lactic acid (0.5, 2.5, 4.7, 6.6 or 8.5×10^{-2} M) was placed into a closed 100 ml glass vessel and heated at 100 °C for 24 h. The solid product was separated from the mother liquor on a glass filter, washed several times with distilled water and then dried at 50 °C overnight.

Characterisation

Powder X-ray diffraction (XRD) patterns of the samples were recorded on a Bruker D8 Advance diffractometer ($Cu_{K\alpha}$ radiation, Ni-filter, LYNXEYE detector, Bragg–Brentano reflection geometry). The microstructure of the samples was investigated using high-resolution scanning electron microscopy (Carl Zeiss NVision 40 equipped with an Oxford Instruments X-Max EDX detector) at accelerating voltages in the range of 1–10 kV. The yttrium content in the solid samples was determined by reverse complexometric titration.[44] Briefly, the samples were dissolved in an excess of hot EDTA and free EDTA was titrated by magnesium sulfate with Arsenazo I indicator. Carbon, hydrogen and nitrogen content in the samples was determined using a Carlo Erba Instruments EA 1108 CHN analyser. The IR spectra of the samples were recorded on an ALPHA FTIR Spectrometer (Bruker) in the range of 4000–300 cm^{-1}, with a resolution of 0.5 cm^{-1}, in an attenuated total reflection mode. Luminescence spectra of the powders were recorded using a Perkin Elmer LS-55 luminescence spectrophotometer with 0.5 nm resolution, at room temperature. The thermal behaviour of basic yttrium lactate was studied using a combined TGA/DSC/DTA (thermogravimetric analysis/differential scanning calorimetry/differential thermal analysis) analyser SDT Q-600, the samples were heated to a temperature of 800 °C (heating rate of 10° min^{-1}) in an air flow (250 ml min^{-1}).

Crystal data for 1. $C_9H_{19}O_{11}Y$, $F_w = 392.15$, monoclinic, $a = 10.5780(8)$, $b = 5.7390(5)$, $c = 13.2053(10)$ Å, $\beta = 97.765(3)°$, $V = 794.31(11)$ Å^3, space group $P2_1$, $Z = 2$, $D_c = 1.640$ g cm^{-3}, $F(000) = 400$, $\mu(MoK_\alpha) = 3.720$ mm^{-1}, colourless needle sizing *ca.* 0.25 × 0.04 × 0.01 mm. A total of 8780 reflections (3457 unique, $R_{int} = 0.078$) were measured on a Bruker D8 Venture diffractometer (graphite monochromatised MoK_α radiation, $\lambda = 0.71073$ Å) using ω-scan mode at 150 K. Absorption correction based on measurements of equivalent reflections was applied.[45] The structure was solved by direct methods and refined by full matrix least-squares on F^2 with anisotropic thermal parameters for all non-hydrogen atoms.[46] All H atoms were placed in calculated positions and refined using a riding model. The final residuals were: $R_1 = 0.0667$, $wR_2 = 0.1523$ for 3175 reflections with $I > 2\sigma(I)$ and 0.0727, 0.1561 for all data and 190 parameters.

Flack parameter = −0.009(6), GoF = 1.121, maximum $\Delta\rho$ = 2.148 e Å^{-3}. The crystallographic data for **1** have been deposited with the Cambridge Crystallographic Data Centre as ESI publications under CCDC number 2085515.†

SEM, CHN, powder and single crystal X-ray diffraction measurements were performed using the equipment of the Joint Research Centre for Physical Methods of Research at Kurnakov Institute of General and Inorganic Chemistry of the Russian Academy of Sciences (JRC PMR IGIC RAS).

Small angle neutron scattering (SANS) investigations were performed using the YuMO time-of-flight spectrometer at the IBR-2 pulsed reactor (Dubna, Moscow region, Russia). Standard data acquisition time per sample was 30 min. Two ring wire He^3-detectors[47] at distances of 4 m and 13 m from the sample position were used in the experiment. Scattered intensity (differential cross section per sample volume) was measured as a function of the momentum transfer modulus $q = (4\pi/\lambda)\sin(\theta/2)$, where θ is the scattering angle and λ is the incident neutron wavelength. An incident neutron beam distribution provided an available wavelength range of 0.5–8 Å, which corresponds to a momentum transfer (q) range of 0.007–0.3 Å^{-1}. The raw data were treated using SAS software.[48] The raw SANS data were converted to an absolute scale by normalisation to the incoherent scattering cross section of a standard vanadium sample. The data were corrected taking account of scattering from the setup and the empty cell. The corrected small-angle neutron scattering curves were presented using an absolute scale with background subtraction.[49]

Results and discussion

Low-temperature hydrothermal treatment (100 °C) of the solutions containing yttrium chloride (1.7 × 10^{-2} M), HMT (2.4–6.6 × 10^{-2} M) and L-lactic acid (0.5–8.3 × 10^{-2} M) resulted in the formation of several different solid products (Fig. 1). At low lactic acid concentrations (0.005 M), white precipitates were formed; at high lactic acid concentrations (0.08 M), needle-like, whitish crystals 1 cm length and a few millimetres thick were obtained. At intermediate lactic acid concentrations (0.025–0.065 M), the synthesis resulted in the formation of white, monolithic gels.

Fig. 2 shows typical powder X-ray diffraction patterns of the samples prepared from the reaction mixtures containing various amounts of L-lactic acid. Hydrolysis of yttrium chloride in the presence of a small amount (0.005 M) of lactic acid resulted in an X-ray amorphous powder. The position of the maximum of the halo (9–10° 2θ) in its diffraction pattern (Fig. 2a) indicates a probable short-range ordering (~10 Å) in the amorphous compound obtained. The X-ray diffraction pattern of the powder prepared with a higher lactic acid concentration (0.047 M) contained three wide, low-angle diffraction maxima (5.8°, 7.4°, 8.9° 2θ), indicating low crystallinity of this product and corresponding to interlayer distances of ~15, 12 and 10 Å (Fig. 2b). These diffraction peaks cannot be attributed to any known crystalline substance. At higher L-lactic acid concentrations in the reaction mixtures (0.08 M), a previously unknown crystalline compound **1** was formed (Fig. 2c).

While rare earth lactate complexes in the solutions have been extensively studied,[25,30–34] to date, no crystal structures of rare earth lactates have been reported. Only layered structure of $[Ln(Lac)_2](H_2O)_2[ClO_4]$ (Ln = Eu and Tb) complex,[36,37] is known. This compound comprises host cationic $Ln(Lac)_2$ layers and interlayer perchlorate ions connected to the host through hydrogen bonds.

For the single crystal experiments, more than ten crystals of compound **1** were examined and all of them exhibited a twinned nature (tripled or sextupled initial cell volumes, unstable and inaccurate cell dimensions refinement). In all the cases, attempts to resolve the twinning using APEX3 software[50] failed because the close proximity of diffraction peaks resulted in the instability of integration procedures. To obtain crystals of better quality, several attempts were made to re-crystallise compound **1** from different organic solvents (methanol, DMSO, DMF) and all of them failed due to the low solubility of the compound. For

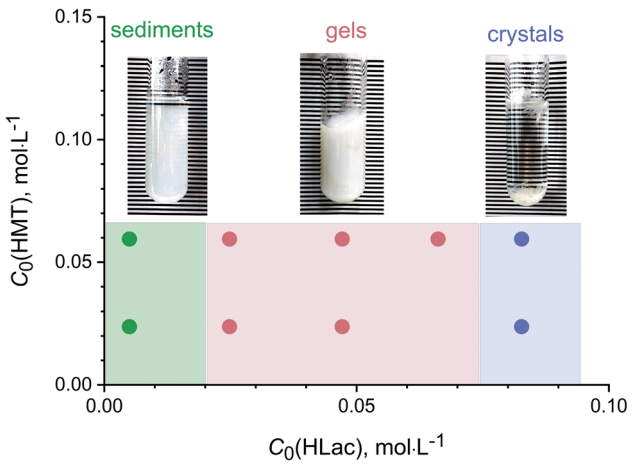

Fig. 1 The products formed upon low-temperature hydrothermal treatment of solutions containing yttrium chloride (1.7 × 10^{-2} M), HMT (0.024, 0.066 M) and L-lactic acid (0.005–0.083 M).

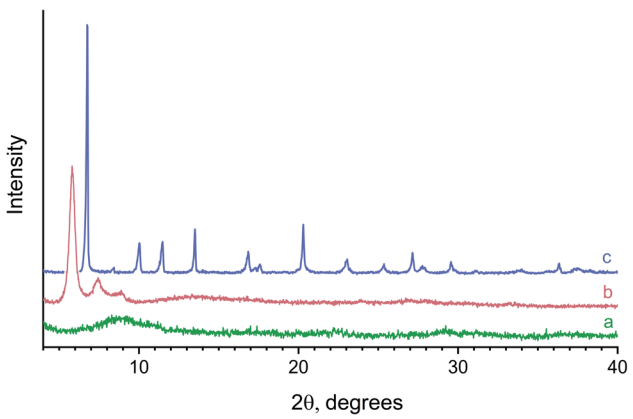

Fig. 2 Powder X-ray diffraction patterns of the solids formed upon hydrothermal treatment of mixed solutions containing yttrium chloride (1.7 × 10^{-2} M), HMT (6.6 × 10^{-2} M) and L-lactic acid (a – 5 × 10^{-3} M, b – 4.7 × 10^{-2} M and c – 8.3 × 10^{-2} M).

all the crystals of compound **1** that were examined, the best single crystal data resulted in $Y(C_3H_5O_3)_3(H_2O)_2$ (sp. gr. $P2_1$), $a = 10.5780(8)$, $b = 5.7390(5)$, $c = 13.2053(10)$ Å, $\beta = 97.765(3)°$, $V = 794.31(11)$ Å^3, $Z = 2$ (Fig. S1†). According to the Cambridge Structural Database, compound **1** is the first structurally characterised yttrium lactate.

The molecule of **1** is monomeric, with an yttrium coordination number equal to 8 (Fig. 3). The coordination environment of the central atom is formed by three η^2-lactate ligands and two water molecules in *cis*-positions to each other, with an O_w–Y–O_w angle equal to 70.6(3)°. The resulting structural data (see Table 1) agree well with the theoretical calculations made by Roy *et al.* for the structure of lanthanum lactate complexes including $La(Lac)_3(H_2O)_2$.[33] The predicted interatomic distances for La–$O_{carboxylate}$, La–$O_{\alpha\text{-hydroxy}}$ and La–O_{water} in the complex were 2.48 ± 0.03 Å, 2.65 ± 0.11 Å and 2.23 ± 0.44 Å;[33] the differences between these values and the values presented in Table 1 are

Table 1 Selected bond lengths (Å) and angles (°) for compound **1**

Y(1)–O(11)	2.296(9)	O(1)–Y(1)–O(2)	70.6(3)
Y(1)–O(21)	2.316(9)	O(11)–Y(1)–O(13)	66.9(3)
Y(1)–O(31)	2.323(9)	O(21)–Y(1)–O(23)	65.0(3)
Y(1)–O(13)	2.325(9)	O(31)–Y(1)–O(33)	65.3(3)
Y(1)–O(23)	2.369(9)		
Y(1)–O(33)	2.390(9)		
Y(1)–O(1)	2.324(9)		
Y(1)–O(2)	2.368(8)		

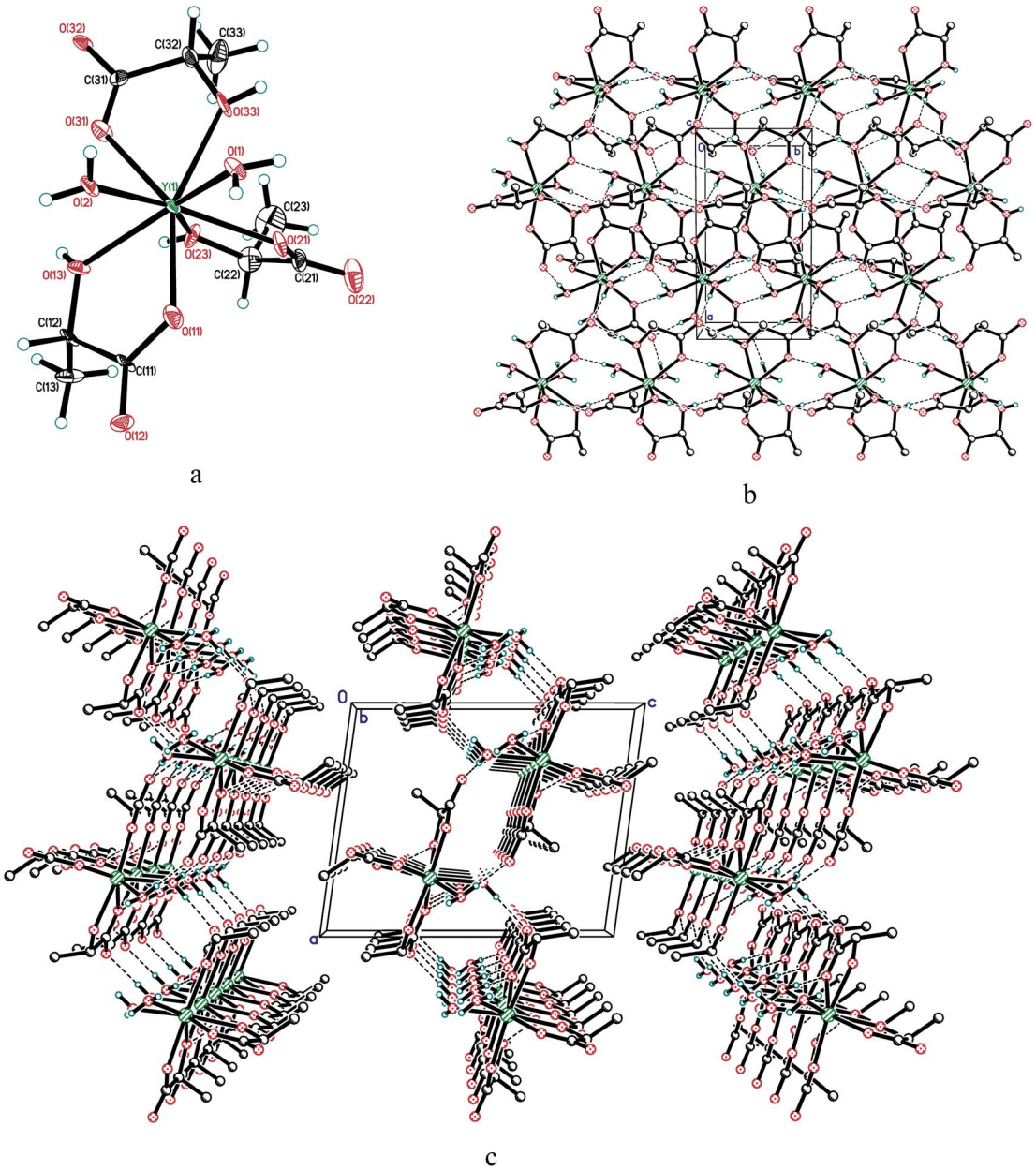

Fig. 3 (a) Molecular structure of **1**; displacement ellipsoids are shown at 50% probability level. (b) Hydrogen bonded layer in the structure of **1**, viewed along the *c*-axis and (c) the *b*-axis.

obviously due to the differences in lanthanum and yttrium atomic radii, as well as to the consideration of outer sphere water molecules in the calculations made by Roy *et al.*[33]

Both Y ← O_w distances (2.324(9) and 2.368(8) Å) lie within the range 2.276–2.652 Å that appears in the Cambridge Structural Database (ver. 5.42, November 2020 (ref. 51)) for terminal water molecules in yttrium complexes with CN = 8 (157 error-free, non-disordered entries, 450 fragments, mean 2.363 Å). The lengths of dative bonds Y ← O(H)C (2.325(9)–2.390(9) Å) are also typical for yttrium (CN = 8) compounds (2.277–2.474 Å for 28 accurate entries with 42 fragments, mean 2.381 Å). All five-membered metallocycles are planar within 0.03 Å.

As expected, Y–OC(=O) bonds are the shortest within the polyhedra (see Table 1). Interestingly, in lactate anions, the longer the Y–OC(=O) bond is, the longer the Y ← O(H)C distance is. This may indicate the active involvement of the α-hydroxy group in the coordination with yttrium. Generally, the contribution of the α-hydroxy group to the coordination of yttrium by the lactate anion is actively debated in the literature. Tian *et al.* reasoned that the participation of α-hydroxy oxygen atoms in the coordination of rare earths promotes the increased stability of Ln(III) lactate complexes.[24] Depending on which model is used, either protonated or deprotonated α-hydroxy groups were considered to enter the coordination sphere of rare earth atoms, the hydrogen bonding of the α-hydroxy group with a water molecule playing an important role.[24,25,33]

In compound **1**, all active hydrogen atoms of α-hydroxy groups and water molecules are involved in intermolecular hydrogen bonding, with O···O distances ranging within 2.642(13)–2.839(12) Å. They combine adjacent molecules in the layer perpendicular to the *c*-axis (Fig. 3).

Comparison of single crystal diffraction data collected at 150 K and the powder X-ray diffraction pattern collected at 298 K enabled an estimate to be made of thermal expansion coefficients for lattice parameters of compound **1**, $\alpha_a = \frac{1}{a}\frac{\Delta a}{\Delta T} = 7.7 \times 10^{-5}\ K^{-1}$; $\alpha_b = \frac{1}{b}\frac{\Delta b}{\Delta T} = 2.6 \times 10^{-5}\ K^{-1}$; $\alpha_c = \frac{1}{c}\frac{\Delta c}{\Delta T} = 3.9 \times 10^{-5}\ K^{-1}$; $\alpha_\beta = \frac{1}{\beta}\frac{\Delta \beta}{\Delta T} = 5.3 \times 10^{-6}\ K^{-1}$; $\alpha_V = \frac{1}{V}\frac{\Delta V}{\Delta T} = 1.4 \times 10^{-4}\ K^{-1}$.

The chemical composition of compound **1**, as determined by CHN analysis and complexometric titration (Table 2), corresponds well with the chemical composition determined using single-crystal diffraction. The chemical composition of compound **1** agrees well with the lanthanum lactate complex $La(Lac)_3(H_2O)_2$ predicted by Roy *et al.*,[33] where the lanthanum first coordination sphere includes two water molecules and three lactate anions having bidentate coordination (by carboxylate and protonated α-hydroxy group).[24]

In their recent report, Powell and Farrell[26] hypothesised the formation of yttrium lactate dihydrate, $Y(Lac)_3 \cdot 2H_2O$, as a result of low-temperature (100 °C) thermal decomposition of $Y(Lac)_3 \cdot 3H_2O$ in air. It is assumed that, in experiments carried out for the current study, upon low-temperature hydrothermal treatment, a moderately soluble yttrium lactate trihydrate can form, which subsequently loses a water molecule and transforms to $Y(Lac)_3(H_2O)_2$. Nevertheless, the exact mechanism of the formation of yttrium lactates under hydrothermal conditions needs further refinement.

Table 2 Results of the chemical analysis of the solid products formed upon hydrothermal treatment of mixed solutions of yttrium chloride (1.7×10^{-2} M), HMT (6.6×10^{-2} M) and L-lactic acid (4.7×10^{-2} M or 8.3×10^{-2} M)

L-Lactic acid concentration in the reaction mixture, M	Solid product formed	Content [wt%] Measured	Calculated
8.3×10^{-2}	Yttrium lactate, **1** $Y(C_3H_5O_3)_3(H_2O)_2$	Y 23.0	Y 22.7
		C 27.9	C 27.6
		H 5.1	H 4.9
		O 44.0	O 44.9
4.7×10^{-2}	'$Y_4(OH)_5(C_3H_5O_3)_7 \cdot 6H_2O$'	Y 30.6	Y 30.3
		C 21.6	C 21.5
		H 4.5	H 4.5
		O 43.3	O 43.7

With moderate L-lactic concentrations in the reaction mixtures, upon low-temperature hydrothermal treatment, the formation of monolithic gels was observed. When the gels were filtered on a glass filter, followed by washing and ambient drying, they flattened and formed paper-like, foldable, solid substances (see Fig. 4).

The gelation of yttrium-containing compounds is quite an unusual phenomenon. Initially, it was supposed that the gels were formed due to the polycondensation of L-lactic acid catalysed by yttrium ions, since REE compounds were reported to catalyse this reaction.[52,53] However, IR-spectroscopy data did not confirm this hypothesis. The absence of the most intense absorption bands characteristic of mono- (1770 cm^{-1}, cyclic dilactone C=O valence vibration) or polylactides (1757 cm^{-1}, valence vibration of C=O of aliphatic esters)[54] indicated the absence of lactide moieties in the compounds obtained. In Fig. 5, one can see that the IR spectra of crystalline yttrium lactate **1** and the paper-like material are almost identical. Within the 3500–3000 cm^{-1} range, OH valence vibrations of

Fig. 4 Appearance of a paper-like material obtained upon the filtering of the gels formed by the low-temperature hydrothermal treatment of reaction mixtures containing yttrium chloride (1.7×10^{-2} M), HMT (6.6×10^{-2} M) and L-lactic acid (4.7×10^{-2} M).

lactate ions, water molecules and hydroxide groups are observed. The most intense lines in the spectrum are located at ~1580, 1400 and 1100 cm^{-1}, indicating the symmetric vibrational modes of the COO^- group, anti-symmetric vibrational modes of the COO^- group and valence vibrational modes of the alcoholic C–OH group. These values are in a good agreement with the literature data for metal lactates[55] and NpO_2^+ lactate complexes.[56] Thus, a paper-like material is also an yttrium lactate, probably of a different chemical composition. This supposition is in line with the chemical analysis data (see Table 2).

The difference in IR-spectra of crystalline yttrium lactate **1** and a paper-like material is manifested in the broadening of ν(OH) bands (~3500 cm^{-1}), which indicates a more developed network of hydrogen bonds in the latter substance. The presence of vibrational bands at ~1480 cm^{-1} (deformational modes of $-CH_2-$ or $-CH_3$ groups), ~1275 cm^{-1} (deformational modes of alcoholic OH groups) and 650 cm^{-1} (deformational modes of C–COH group) in **1**, and their absence in IR spectrum of a paper-like material, indicates the higher crystallinity of the former compound and the diversity in coordination modes of lactate alcoholic OH-groups in the latter compound. The differences in spectra are also observed within a low frequency region (350–800 cm^{-1}), where a wide absorption band at ~700 cm^{-1} for the paper-like material can be attributed to Y–O valence vibrations.

A detailed analysis of the IR spectrum of the paper-like material (the splitting of antisymmetric and symmetric stretching modes of the carboxylic groups) made it possible to determine a coordination type of carboxylic groups in lactate ligands to Y^{3+} cations.[56] Generally, a bidentate coordination of carboxylic groups of lactate ligands is accompanied by a smaller spectral splitting (≤100 cm^{-1}), whereas a monodentate binding results in a larger spectral splitting (≥150 cm^{-1}).[56,57] The splitting of antisymmetric and symmetric stretching modes in the spectra of crystalline yttrium lactate and the paper-like material were 187 cm^{-1} and 169 cm^{-1}, respectively, indicating monodentate coordination of carboxylic groups of a lactate ligand to Y^{3+} cations in both cases. A slightly lower splitting value for the paper-like material may indicate the presence of bridging lactate ligands. A monodentate coordination of carboxyl moiety of the lactate ligand indirectly indicates that the α-hydroxy group enters the coordination sphere of yttrium, which is in good accordance with single crystal data for compound **1**.

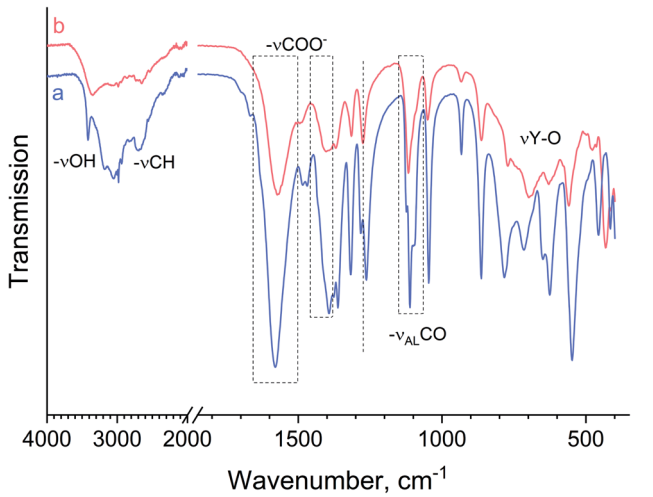

Fig. 5 IR spectra of solids formed during low-temperature hydrothermal treatment of yttrium chloride (1.7×10^{-2} M), HMT (6.6×10^{-2} M) and L-lactic acid (a – 4.7×10^{-2} M; b – 8.3×10^{-2} M). AL – vibrational modes of alcoholic groups.

The chemical composition of the paper-like material can be hypothesised based on general principles governing the formation of yttrium compounds in aqueous media. Compound **1** crystallised from the reaction mixtures at pH ~ 4.5, while the gels were obtained at higher pH values, *i.e.* ~5.5. This difference in pH was obviously due to the different concentration of L-lactic acid, given that in the latter case it was approximately two times lower. At pH values higher than 5, a hydrolysis of yttrium cations occurs and the formation of Y–OH moieties becomes likely and might even become uncontrollable.[58] However, at relatively high pH, multidentate ligands are known to limit Y^{3+} hydrolysis. Within a 'ligand controlled hydrolysis' approach,[59] different polynuclear rare earth hydroxy complexes can be obtained, bearing amino carboxylate ligands.[60] In particular, rare earth amino carboxylates often comprise cubane tetranuclear $[REE_4(\mu_3\text{-}OH)_4]^{8+}$ units.[19] Interestingly, at nearly neutral pH (~6) and under mild hydrothermal conditions, the interaction of rare earth ions with mono- or bidentate ligands can result in polynuclear coordination compounds, which are often regarded as layered rare earth hydroxides (LRHs) comprising infinite positively charged 2D layers of $[RE(OH)_{3-n}]^{n+}$ bonded by the ligands into laminate structures.[61–63] These ion-exchangeable and exfoliatable substances have a great deal of flexibility in terms of their chemical composition[61,64–66] and are now regarded as a basis for promising bioactive theranostic materials.[67,68] From the findings of the current study, a paper-like material couldn't be classified as a layered rare earth hydroxide as the positions of the maxima in its diffraction pattern (see Fig. 2) are incompatible with the LRHs' structure.

Thus, it can be concluded from the current study that, at relatively high pH values and under low-temperature hydrothermal conditions, the hydrolysis of yttrium cations controlled by multidentate lactate ligands results in the formation of oligonuclear yttrium hydroxy lactate. Unfortunately, the work was unsuccessful in obtaining single crystals under corresponding synthetic conditions, since all the compounds synthesised had a semi-amorphous nature, having wide, small-angle maxima in their diffraction patterns (see Fig. 2).

Taking into account all the above considerations and the experimental data for the paper-like material, its chemical composition can be hypothesised as a basic yttrium lactate, $Y_4(OH)_5(C_3H_5O_3)_7 \cdot 6H_2O$. Thus, its precipitation can be described as follows:

$$4Y^{3+} + 3C_6N_4H_{12} + 7C_3H_6O_3 + 29H_2O \rightarrow Y_4(OH)_5(C_3H_5O_3)_7 \cdot 6H_2O + 18H_2CO + 12NH_4^+ \quad (1)$$

Thermal analysis data corroborate the hypothesised composition of basic yttrium lactate well (Fig. 6). After heating in air, the paper-like material showed multi-stage decomposition behaviour. The first stage of thermal decomposition (up to 100 °C) was obviously due to the removal of physically bound water. The second decomposition stage (200–500 °C) was more complex and included the removal of a chemically bound water substage (100–260 °C). The weight loss (~9.6 wt%) in this temperature range corresponds well to the removal of 8.5 water molecules per $Y_4(OH)_5(C_3H_5O_3)_7 \cdot 6H_2O$ formula unit, yielding anticipated anhydrous yttrium oxidolactate $Y_4O_{2.5}(Lac)_7$. At higher temperatures (up to 500 °C), the oxidation of lactate moieties occurs, probably yielding various carbonates such as $Ln(C_3H_5O_3)CO_3$, $Ln_2(CO_3)_3$ or $Ln_2O(CO_3)_2$.[26] The oxidation of organic matter in the paper-like material was also indicated by a pronounced exothermic effect (maximum at 343 °C) in the DSC curve. Interestingly, the maximum rate of lactate moiety decomposition in air (~370 °C) is observed at much higher temperatures than the maximum rate of pure lactic acid thermolysis in nitrogen flow (180–240 °C) reported by Komesu *et al.*[69] The final decomposition stage (500–800 °C) of the paper-like material can be attributed to the decomposition of residual carbon-containing matter and the formation of yttrium oxide.

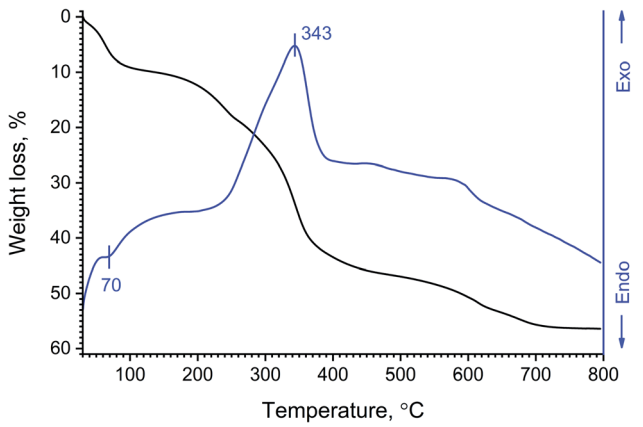

Fig. 6 Weight loss and DSC curves of the paper-like material formed as a result of hydrothermal treatment of yttrium chloride (1.7×10^{-2} M), HMT (6.6×10^{-2} M) and L-lactic acid (4.7×10^{-2} M) solution mixtures.

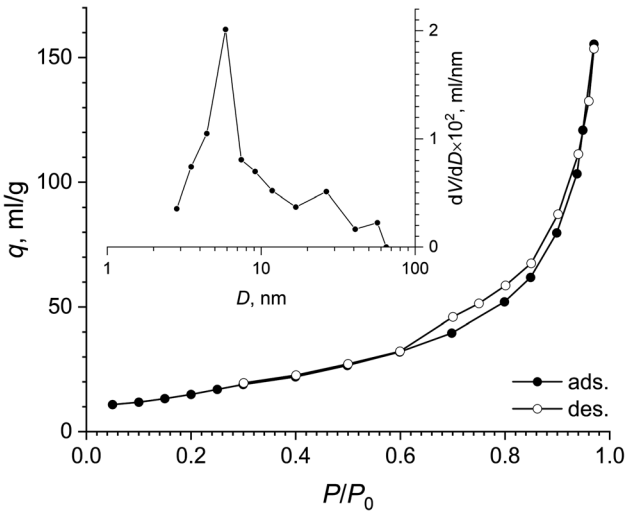

Fig. 8 Full nitrogen adsorption–desorption isotherm and pore size distribution (inset) for the paper-like sample.

The thermal analysis data seem to be similar to those obtained by Powell and Farrell[26] for hypothetical yttrium lactate trihydrate, $Y(Lac)_3 \cdot 3H_2O$, yet, in their report, they presented neither the results of chemical analysis of the compounds obtained, nor thermal analysis curves.

One very special feature of the paper-like material was its microstructure (see Fig. 7). It consisted of fibres with an average thickness varying from 10 to 80 nm, depending on the lactic acid content of the reaction mixture (see ESI, Fig. S2†). These data are in good agreement with the particle size estimates using the Scherrer equation for the X-ray diffraction data, ~25 nm (see Fig. 2b). According to observations derived from the current study, the concentration of HMT did not significantly affect fibre thickness. Such a microstructure obviously provides the material with superior mechanical properties, *i.e.* its flexibility and foldability.

Thus, basic yttrium lactate can be classified as a 1D material composed of interlaced fibres. Interestingly, direct sol–gel methods for the synthesis of 1D gels of complex metal compounds are virtually unknown. The scarce examples of sol–gel derived 1D gels are vanadium pentoxide gels obtained from

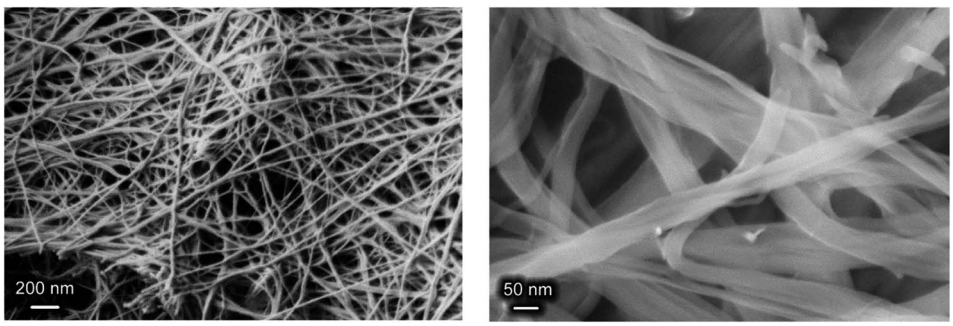

Fig. 7 SEM images of a paper-like material formed as a result of the hydrothermal treatment of yttrium chloride (1.7×10^{-2} M), HMT (6.6×10^{-2} M) and L-lactic acid (4.7×10^{-2} M) solution mixtures.

Table 3 Structural parameters of basic yttrium lactate paper-like material derived from SANS data

Parameter	$G \times 10^2$, cm^{-1} $Å^{-s}$	s	R_g, Å	$A \times 10^7$, cm^{-1} $Å^{-n_2}$	n_2	$B \times 10^4$, $Å^{-n_1}$	n_1
Value	4 ± 0.5	1.95 ± 0.08	85 ± 7	1.8 ± 0.4	3.98 ± 0.02	2 ± 0.2	2.09 ± 0.10

neutral $VO(OH)_3$ species or vanadium alkoxide precursors[70] and ceric hydrogen phosphate gels derived from CeO_2 solutions in orthophosphoric acid.[71,72] It is possible that the fibres in these gels form according to a polymeric growth mechanism, but the exact mechanism of 1D gel formation needs further clarification.

To assess the microstructure of basic yttrium lactate, low-temperature nitrogen adsorption measurements and small-angle neutron scattering experiments were performed, the latter technique being common in the study of the structure of amorphous or semi-amorphous materials.[73]

According to low-temperature nitrogen adsorption data, the paper-like basic yttrium lactate had a high specific surface area, of 75 m^2 g^{-1}. Fig. 8 shows the full nitrogen adsorption/desorption isotherm for the sample. The isotherm has a narrow hysteresis loop, which can be attributed to the H3 type, according to the IUPAC classification,[74] indicating the presence of slit-like mesopores in the sample. The pore size distribution calculated using the BJH model indicates the presence of mesopores in the material, with the maximum at ~6 nm.

Fig. S3† presents a small-angle neutron scattering curve for the basic yttrium lactate sample. The shape of the curve is typical of disordered porous systems containing two types of scatterer of different size.[75–77] The exponent values calculated from the slope of the straight-line sections of the experimental $\log\left(\frac{d\Sigma(q)}{d\Omega}\right) \sim \log(q)$ curves were $n_1 = 2.09 \pm 0.10$ and $n_2 = 3.98 \pm 0.02$. The n_1 value indicates that the system consisted of randomly oriented flattened particles.[73] Unfortunately, the geometrical parameters of these particles cannot be correctly estimated from the neutron scattering experimental data, since the contributions of these parameters interfere with the contribution from the structural characteristics of the aggregates of these particles.

The value of $n_2 \approx 4$ (Porod scattering law[78]) indicates that particle aggregates possess an almost smooth surface, the surface fractal dimension being $D_S = 2.02 \pm 0.02$. The characteristic size of these aggregates R_c can be estimated from the low q region of the curve ($q < 1 \times 10^{-2}$ $Å^{-1}$) corresponding to the transition from the Porod to the Guinier regime.[79] To fit all of the experimental data, the following model was used:

$$\left.\begin{aligned} \frac{d\Sigma(q)}{d\Omega} &= \frac{G}{q^s}\exp\left(-\frac{q^2 R_g^2}{3-s}\right), \quad q \le 0.01 \ \text{Å}^{-1} \\ \frac{d\Sigma(q)}{d\Omega} &= \frac{A}{q^{n_2}} + \frac{B}{q^{n_1}}, \quad q \ge 0.01 \ \text{Å}^{-1} \end{aligned}\right\} \quad (2)$$

Here, parameter s is responsible for the shape of the particles: $s = 0$ for spheres, $s = 1$ for fibrillae, $s = 2$ for lamellae; R_g – gyration radius of the scattering objects; G – Guinier coefficient;[79] A and B – coefficients indicating the local structure of scattering objects.[80] The results of the fitting process are presented in Fig. S3† and Table 3.

The values presented in Table 3 indicate that the paper-like sample consisted of thin ribbons ($s \approx 2$) with a smooth surface ($D_s = 2.02 \pm 0.02$) and a thickness of $\sqrt{12}R_g \approx 30$ nm. It should be noted that this value is an upper-bound estimate. Nevertheless, this value is in good agreement with SEM data for the corresponding sample which had an average particle size of 33 nm (see Fig. 7). In turn, the X-ray diffraction pattern of basic yttrium lactate paper (see Fig. 2b) shows reflections corresponding to 1–2 nm interplanar distances. Taking into account low-temperature nitrogen adsorption data, indicating the presence of slit-like pores with a size of ~6 nm, the structure of fibrillae which form the basic yttrium lactate paper-like material can be hypothesised (see Fig. 9).

Thin particles in the structure of basic yttrium lactate are advantageous for the preparation of ultra-small rare earth oxide nanoparticles *via* the thermal decomposition or combustion of this compound. The annealing of basic yttrium lactate paper in air at temperatures up to 800 °C were performed during the

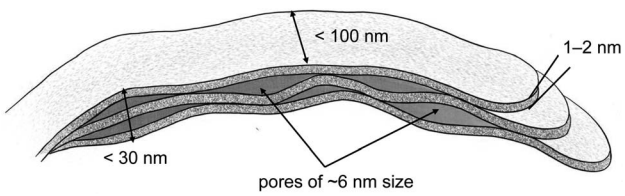

Fig. 9 The structure of basic yttrium lactate fibres, as hypothesised from low-temperature nitrogen adsorption, small-angle neutron scattering and scanning electron microscopy data.

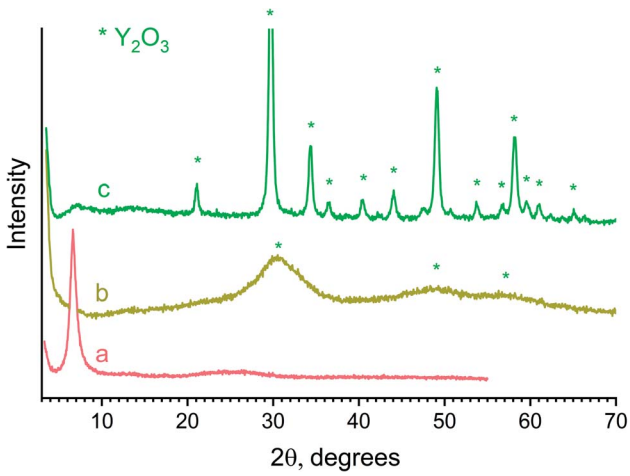

Fig. 10 X-ray diffraction patterns of a paper-like material annealed at (a) 120, (b) 450, (c) 800 °C.

current study. After heating, the material changed its colour from beige (120 °C) to brown (450 °C) and white (800 °C). The sample annealed at 450 °C for 1 h consisted of nanocrystalline Y_2O_3, having 3 nm size, as estimated using the Scherrer equation. At 800 °C, the particle size increased to 21 nm, due to the coarsening of nanoparticles (see Fig. 10). The synthesis of ultrasmall yttria nanoparticles is of special interest in view of their wide potential for biomedical applications.[81,82] To date, there have been many attempts to prepare yttria nanoparticles using the sol–gel technique (*e.g.* ref. 82 and 83), with only a few of them succeeding in the preparation of yttria powders with a crystal size smaller than 10 nm (*e.g.* ref. 84 and 85).

Conclusions

A first successful attempt has been made to synthesise a crystalline molecular yttrium lactate complex ($Y(Lac)_3(H_2O)_2$), where the coordination sphere of yttrium was saturated with lactate ligands and water molecules, resulting in a neutral molecular moiety. In a crystal structure, these molecular complexes were interconnected in 2D layers by hydrogen bonds between α-hydroxy groups of lactate ligands and water molecules. The use of similar reaction mixtures containing higher amounts of L-lactic acid, and hence having a higher pH, enabled the synthesis of a paper-like material comprising basic yttrium lactate with the supposed composition '$Y_4(OH)_5(C_3H_5O_3)_7 \cdot 6H_2O$'. This material consisted of flattened interwoven fibres with a width of ~30 nm, which account for the flexibility and foldability of the material. The synthesised substances are the first representatives of solid state rare earth lactates.

Funding

The work was supported by the Ministry of Science and Higher Education of the Russian Federation (grant agreement no. 075-15-2020-782).

Conflicts of interest

There are no conflicts to declare.

Acknowledgements

The graphical abstract was created using Biorender.com.

References

1 S. Yuan, L. Feng, K. Wang, J. Pang, M. Bosch, C. Lollar, Y. Sun, J. Qin, X. Yang, P. Zhang, Q. Wang, L. Zou, Y. Zhang, L. Zhang, Y. Fang, J. Li and H. Zhou, *Adv. Mater.*, 2018, **30**, 1704303.
2 S. V. Eliseeva and J.-C. G. Buenzli, *Chem. Soc. Rev.*, 2010, **39**, 189–227.
3 R. Janicki, A. Mondry and P. Starynowicz, *Coord. Chem. Rev.*, 2017, **340**, 98–133.
4 A. J. Amoroso and S. J. A. Pope, *Chem. Soc. Rev.*, 2015, **44**, 4723–4742.
5 J. Wang, M. Feng, M. N. Akhtar and M.-L. Tong, *Coord. Chem. Rev.*, 2019, **387**, 129–153.
6 S. Roy, A. Chakraborty and T. K. Maji, *Coord. Chem. Rev.*, 2014, **273–274**, 139–164.
7 A. A. Sidorov, N. V. Gogoleva, E. S. Bazhina, S. A. Nikolaevskii, M. A. Shmelev, E. N. Zorina-Tikhonova, A. G. Starikov, M. A. Kiskin and I. L. Eremenko, *Pure Appl. Chem.*, 2020, **92**, 1093–1110.
8 M. Du, C.-P. Li, C.-S. Liu and S.-M. Fang, *Coord. Chem. Rev.*, 2013, **257**, 1282–1305.
9 A. S. Pronin, S. A. Semenov, D. V. Drobot, E. V. Volchkova and G. I. Dzhardimalieva, *Russ. J. Inorg. Chem.*, 2020, **65**, 1173–1185.
10 M. Sertçelik and M. Durman, *Russ. J. Inorg. Chem.*, 2020, **65**, 1351–1359.
11 J. Lu and R. Wang, in *Encyclopedia of Inorganic and Bioinorganic Chemistry*, John Wiley & Sons, Ltd, Chichester, UK, 2012.
12 I. P. Stolarov, N. V. Cherkashina, I. A. Yakushev, A. V. Churakov, A. B. Kornev and E. V. Fatyushina, *Russ. J. Inorg. Chem.*, 2020, **65**, 507–513.
13 R. D. Shannon, *Acta Crystallogr., Sect. A: Cryst. Phys., Diffr., Theor. Gen. Crystallogr.*, 1976, **32**, 751–767.
14 *Rare Earth Coordination Chemistry*, ed. C. Huang, John Wiley & Sons, Ltd, Chichester, UK, 2010.
15 P. Halder, B. Chakraborty, P. R. Banerjee, E. Zangrando and T. K. Paine, *CrystEngComm*, 2009, **11**, 2650.
16 J. Yang, C. A. Trickett, S. B. Alahmadi, A. S. Alshammari and O. M. Yaghi, *J. Am. Chem. Soc.*, 2017, **139**, 8118–8121.
17 J. Wahsner, E. M. Gale, A. Rodríguez-Rodríguez and P. Caravan, *Chem. Rev.*, 2019, **119**, 957–1057.
18 F. Nawaz, H. Cao, Y. Xie, J. Xiao, Y. Chen and Z. A. Ghazi, *Chemosphere*, 2017, **168**, 1457–1466.
19 Z. Zheng, in *Encyclopedia of Inorganic and Bioinorganic Chemistry*, John Wiley & Sons, Ltd, Chichester, UK, 2012.
20 M. Nalbandian and M. Takeda, *Biology*, 2016, **5**, 38.
21 M. Adeva-Andany, M. López-Ojén, R. Funcasta-Calderón, E. Ameneiros-Rodríguez, C. Donapetry-García, M. Vila-Altesor and J. Rodríguez-Seijas, *Mitochondrion*, 2014, **17**, 76–100.
22 K. L. Nash, G. Johnson, D. Brigham, C. Marie, T. S. Grimes and J. C. Braley, *Procedia Chem.*, 2012, **7**, 45–50.
23 K. L. Nash, *Solvent Extr. Ion Exch.*, 2015, **33**, 1–55.
24 G. Tian, L. R. Martin and L. Rao, *Inorg. Chem.*, 2010, **49**, 10598–10605.
25 A. Barkleit, J. Kretzschmar, S. Tsushima and M. Acker, *Dalton Trans.*, 2014, **43**, 11221–11232.
26 J. E. Powell and J. L. Farrell, *Some Observations regarding rare-earth lactates*, Ames, IA (United States), 1962.
27 M. Sakanoue and M. Nakatani, *Bull. Chem. Soc. Jpn.*, 1972, **45**, 3429–3433.
28 M. A. Gouveia and R. G. de Carvalho, *J. Inorg. Nucl. Chem.*, 1966, **28**, 1683–1688.
29 G. R. Choppin, *Pure Appl. Chem.*, 1971, **27**, 23–42.
30 G. R. Choppin and J. A. Chopoorian, *J. Inorg. Nucl. Chem.*, 1961, **22**, 97–113.
31 P. G. Manning, *Can. J. Chem.*, 1965, **43**, 3258–3263.

32 A. Skerencak-Frech, F. Taube, P. L. Zanonato, M. Acker, P. J. Panak and P. Di Bernardo, *Thermochim. Acta*, 2019, **679**, 178316.
33 L. E. Roy and L. R. Martin, *Dalton Trans.*, 2016, **45**, 15517–15522.
34 T. S. Grimes, M. A. Nilsson and K. L. Nash, *Sep. Sci. Technol.*, 2010, **45**, 1725–1732.
35 Y. Li, P. Yan, G. Hou, H. Li, P. Chen and G. Li, *J. Organomet. Chem.*, 2013, **723**, 176–180.
36 Z.-R. Qu, Q. Ye, H. Zhao, D.-W. Fu, H.-Y. Ye, R.-G. Xiong, T. Akutagawa and T. Nakamura, *Chem.–Eur. J.*, 2008, **14**, 3452–3456.
37 Q. Ye, D.-W. Fu, H. Tian, R.-G. Xiong, P. W. H. Chan and S. D. Huang, *Inorg. Chem.*, 2008, **47**, 772–774.
38 H.-J. Chen, X.-Y. Zheng, Y.-R. Zhao, D.-Q. Yuan, X.-J. Kong, L.-S. Long and L.-S. Zheng, *ACS Appl. Electron. Mater.*, 2019, **1**, 804–809.
39 R. S. Dickins, C. S. Love and H. Puschmann, *Chem. Commun.*, 2001, 2308–2309.
40 Y. Qiu, Z. Liu, J. Mou, H. Deng and M. Zeller, *CrystEngComm*, 2010, **12**, 277–290.
41 M. A. Katkova, G. S. Zabrodina, M. S. Muravyeva, A. S. Shavyrin, E. V. Baranov, A. A. Khrapichev and S. Y. Ketkov, *Eur. J. Inorg. Chem.*, 2015, **2015**, 5202–5208.
42 X.-Y. Chen, G. S. Goff, W. C. Ewing, B. L. Scott and W. Runde, *Inorg. Chem.*, 2012, **51**, 13254–13263.
43 C. N. R. Rao, S. Natarajan and R. Vaidhyanathan, *Angew. Chem., Int. Ed.*, 2004, **43**, 1466–1496.
44 S. J. Lyle and M. M. Rahman, *Talanta*, 1963, **10**, 1177–1182.
45 *SADABS-2016/2, Bruker AXS area detector scaling and absorption correction program*, Bruker AXS Inc., Madison, Wisconsin, U.S.A., 2016.
46 G. M. Sheldrick, *Acta Crystallogr., Sect. C: Struct. Chem.*, 2015, **71**, 3–8.
47 A. I. Kuklin, A. K. Islamov and V. I. Gordeliy, *Neutron News*, 2005, **16**, 16–18.
48 A. G. Soloviev, T. M. Soloveva, A. V. Stadnik, A. H. Islamov and A. I. Kuklin, *Communication of JINR*, Dubna, P10-2003-86, 2003, http://wwwinfo.jinr.ru/programs/jinrlib/sas/086(P10-2003-86).pdf.
49 Y. Ishikawa, M. Furusaka, N. Niimura, M. Arai and K. Hasegawa, *J. Appl. Crystallogr.*, 1986, **19**, 229–242.
50 *APEX3 Crystallography Software Suite*, Bruker AXS Inc., Madison, Wisconsin, U.S.A., 2016.
51 C. R. Groom, I. J. Bruno, M. P. Lightfoot and S. C. Ward, *Acta Crystallogr., Sect. B: Struct. Sci., Cryst. Eng. Mater.*, 2016, **72**, 171–179.
52 E. A. Poryvaeva, T. A. Egiazaryan, V. M. Makarov, M. V. Moskalev, D. A. Razborov and I. L. Fedyushkin, *Russ. J. Org. Chem.*, 2017, **53**, 344–350.
53 D. A. Garlotta, *J. Polym. Environ.*, 2001, **9**, 63–84.
54 L. Nikolic, I. Ristic, B. Adnadjevic, V. Nikolic, J. Jovanovic and M. Stankovic, *Sensors*, 2010, **10**, 5063–5073.
55 G. Cassanas, M. Morssli, E. Fabrègue and L. Bardet, *J. Raman Spectrosc.*, 1991, **22**, 409–413.
56 M. M. Maiwald, K. Müller, K. Heim, M. Trumm, N. L. Banik, J. Rothe, K. Dardenne, A. Skerencak-Frech and P. J. Panak, *New J. Chem.*, 2020, **44**, 17033–17046.
57 K. Nakamoto, in *Infrared and Raman Spectra of Inorganic and Coordination Compounds*, John Wiley & Sons, Inc., Hoboken, NJ, USA, 2009, pp. 1–273.
58 E. Bentouhami, G. M. Bouet, J. Meullemeestre, F. Vierling and M. A. Khan, *C. R. Chim.*, 2004, **7**, 537–545.
59 Z. Zheng, *Chem. Commun.*, 2001, 2521–2529.
60 Z. Zheng, in *Cluster Compounds of Rare-Earth Elements*, 2010, pp. 109–239.
61 A. D. Yapryntsev, A. E. Baranchikov and V. K. Ivanov, *Russ. Chem. Rev.*, 2020, **89**, 629–666.
62 A. Yapryntsev, B. Abdusatorov, I. Yakushev, R. Svetogorov, A. Gavrikov, A. Rodina, Y. Fatyushina, A. Baranchikov, Y. Zubavichus and V. Ivanov, *Dalton Trans.*, 2019, **48**, 6111–6122.
63 A. D. Yapryntsev, A. Y. Bykov, A. E. Baranchikov, K. Y. Zhizhin, V. K. Ivanov and N. T. Kuznetsov, *Inorg. Chem.*, 2017, **56**, 3421–3428.
64 A. D. Yapryntsev, K. B. Ustinovich, A. A. Rodina, V. A. Lebedev, O. I. Pokrovskiy, K. E. Yorov, A. V. Gavrikov, A. E. Baranchikov and V. K. Ivanov, *J. Supercrit. Fluids*, 2019, **150**, 40–48.
65 N. Snejko, F. Gándara, J. Perles, M. Á. Monge, E. Gutiérrez-Puebla, B. Gómez-Lor and M. Iglesias, *Angew. Chem., Int. Ed.*, 2006, **45**, 7998–8001.
66 J. Liang, R. Ma and T. Sasaki, in *Structure and Bonding*, ed. M. Yan and D. Wei, 2015, vol. 166, pp. 69–103.
67 S. Eom, G. Choi, H. Nakamura and J.-H. Choy, *Bull. Chem. Soc. Jpn.*, 2020, **93**, 1–12.
68 R. Ju and Q. Gu, *Appl. Organomet. Chem.*, 2018, **32**, e3926.
69 A. Komesu, P. F. Martins Martinez, B. H. Lunelli, J. Oliveira, M. R. Wolf Maciel and R. Maciel Filho, *J. Chem.*, 2017, **2017**, 1–7.
70 J. Livage, *Chem. Mater.*, 1991, **3**, 578–593.
71 T. O. Kozlova, A. E. Baranchikov, D. A. Kozlov, A. V. Gavrikov, G. P. Kopitsa, A. D. Yapryntsev, K. B. Ustinovich, A. Chennevière and V. K. Ivanov, *ACS Omega*, 2020, **5**, 17592–17600.
72 K. E. Yorov, T. O. Shekunova, A. E. Baranchikov, G. P. Kopitsa, L. Almásy, L. S. Skogareva, V. V. Kozik, A. N. Malkova, S. A. Lermontov and V. K. Ivanov, *J. Sol-Gel Sci. Technol.*, 2018, **85**, 574–584.
73 L. A. Feigin and D. I. Svergun, *Structure Analysis by Small-Angle X-Ray and Neutron Scattering*, Springer US, Boston, MA, 1987.
74 M. Thommes, K. Kaneko, A. V. Neimark, J. P. Olivier, F. Rodriguez-Reinoso, J. Rouquerol and K. S. W. Sing, *Pure Appl. Chem.*, 2015, **87**, 1051–1069.
75 M. Lin, R. Klein, H. Lindsay, D. Weitz, R. Ball and P. Meakin, *J. Colloid Interface Sci.*, 1990, **137**, 263–280.
76 D. Fairén-Jiménez, F. Carrasco-Marín, D. Djurado, F. Bley, F. Ehrburger-Dolle and C. Moreno-Castilla, *J. Phys. Chem. B*, 2006, **110**, 8681–8688.
77 J. Hyeon-Lee, G. Beaucage and S. E. Pratsinis, *Chem. Mater.*, 1997, **9**, 2400–2403.
78 G. Porod, *Kolloid-Z.*, 1951, **124**, 83–114.
79 A. Guinier and G. Frournet *Small-Angle Scattering of X-rays*, John Wiley and Sons, Inc., New York, 1955.

80 J. Teixeira, in *On Growth and Form*, Springer Netherlands, Dordrecht, 1986, pp. 145–162.
81 K. S. Tang, *Life Sci.*, 2020, **259**, 118287.
82 G. Rajakumar, L. Mao, T. Bao, W. Wen, S. Wang, T. Gomathi, N. Gnanasundaram, M. Rebezov, M. A. Shariati, I.-M. Chung, M. Thiruvengadam and X. Zhang, *Appl. Sci.*, 2021, **11**, 2172.
83 K. Lebbou, P. Perriat and O. Tillement, *J. Nanosci. Nanotechnol.*, 2005, **5**, 1448–1454.
84 R. M. Krsmanović Whiffen, D. Bregiroux and B. Viana, *Ceram. Int.*, 2017, **43**, 15834–15841.
85 A. D. Yapryntsev, L. S. Skogareva, A. E. Gol'dt, A. E. Baranchikov and V. K. Ivanov, *Russ. J. Inorg. Chem.*, 2015, **60**, 1027–1033.